IEEE Open Journal of Antennas and Propagation

Received XX XXXXXXXX, 2024; revised XX Month, XXXX; accepted XX Month, XXXX; Date of publication XX Month, XXXX; date of current version XX Month, XXXX.

Digital Object Identifier 10.1109/OJAP.2020.1234567

Improving the performance of the phaseless Sources Reconstruction Method for antenna diagnostics and characterization

YURI ÁLVAREZ LÓPEZ[1], MARÍA GARCÍA FERNÁNDEZ[2], MEMBER, IEEE, JAIME LAVIADA MARTÍNEZ[1],AND FERNANDO LAS-HERAS ANDRÉS[1], SENIOR MEMBER, IEEE

[1]Área de Teoría de la Señal y Comunicaciones, Universidad de Oviedo. Edificio Polivalente, Mod. 8, Campus Universitario de Gijón, 33203, Gijón, Spain
[2]Centre for Wireless Innovation, Queen's University Belfast. BT7 1NN, Belfast, United Kingdom

CORRESPONDING AUTHOR: Yuri Álvarez López (e-mail: alvarezyuri@uniovi.es).

This work was supported in part by the Principado de Asturias/Fundación para el Fomento en Asturias de la Investigación Científica Aplicada y la Tecnología (FICYT) through "Ayudas para grupos de investigación de organismos del Principado de Asturias durante el período 2021–2023," under Reference AYUD/2021/51706; in part by the Ministerio de Ciencia e Innovación of Spain, Agencia Estatal de Investigación of Spain, and Fondo Europeo de Desarrollo Regional (FEDER) under Project PID2021-122697OB-I00 ("META-IMAGER"); in part by the Ministerio de Ciencia e Innovación of Spain, Agencia Estatal de Investigación of Spain and the European Union NextGenerationEU/PRTR (Plan de Recuperación, Transformación y Resiliencia) under Project TED2021-131975AI00/AEI/10.13039/501100011033 ("ANTHEM5G"); and in part by the UK Research and Innovation (UKRI) Postdoctoral Fellowship Guarantee for Marie Skłodowska-Curie Actions (MSCA) Postdoctoral Fellowship under Project EP/X022951/1.
Data supporting this study are available at the IEEE Dataport, dataset https://dx.doi.org/10.21227/367s-by40.

ABSTRACT Unmanned Aerial Vehicles (UAV)-based near field (NF) antenna measurement techniques have experienced significant development in recent years thanks to advantages like the capability of in-situ antenna testing under operational conditions. Different approaches have been proposed to tackle the associated challenges: tethered UAVs, capable of direct acquisition of complex NF measurements; indirect acquisition of the phase of the NF using an additional antenna; and iterative retrieval of the phase from the measurement of the NF amplitude at two different surfaces. While the latter is the simplest method in terms of hardware complexity, it is affected by the limitations of iterative phase retrieval methods, like stagnation due to the local minima of the cost function. This contribution explores the possibility of improving the convergence of these iterative phase retrieval methods by reducing the number of unknowns involved in the minimization problem. For this goal, the use of meshless basis functions to characterize the Antenna Under Test (AUT) is proposed. In particular, Fourier expansion and wavelets will be analyzed. An offset reflector antenna, measured at a spherical range in anechoic chamber as well as with a UAV-based antenna measurement system, will be considered for validation purposes.

INDEX TERMS Antenna measurement, Unmanned Aerial Vehicles, antenna diagnostics, near field to far field (NF-FF), amplitude-only measurements, near field (NF) measurements.

I. INTRODUCTION

ANTENNA measurement using Unmanned Aerial Vehicles (UAVs) has become a topic of growing interest due to the potential applications for in-situ assessment of the antenna performance under operational conditions and/or the capability to measure physically large antennas that cannot be fit into an anechoic chamber [1]–[4]. While first UAV-based systems for antenna measurements were conceived to operate in the far field (FF) region of the Antenna Under Test (AUT) [5]–[7], improvements in positioning and georeferring accuracy and UAV capabilities have enabled the introduction of these systems for near field (NF) measurements. This is of special interest in the case of electrically large antennas, where the FF distance would make impractical the direct

acquisition of the three-dimensional (3D) radiation pattern. A proof-of-concept for UAV-based NF antenna measurement was presented in [8], using a tethered UAV and a laser-based guidance system.

From the review of the state-of-the-art, UAV-based NF antenna measurements can be classified into the following strategies:

- Measurement of the amplitude of the NF radiated by the AUT on two or more measurement surfaces around the AUT [9]–[12]. This approach, also known as scalar measurements in the related literature, relies on recovering the phase of the measured NF employing iterative phase retrieval methods. Then, from the measured amplitude and the recovered phase of the NF, antenna diagnostics and/or NF-FF transformation can be conducted.
  Advantages: hardware simplicity, as only a power detector onboard the UAV is required.
  Drawbacks: iterative phase retrieval techniques can be inaccurate (e.g. risk of stagnation in a local minimum). It might require the UAV to fly at those different measurement surfaces, increasing acquisition time.
- Use of a reference antenna placed in the vicinity of the AUT to create a controlled interference, usually referenced to as hologram, so that the phase of the NF can be retrieved through simple processing [13]–[15].
  Advantages: the recovered phase can be more accurate than iterative phase retrieval methods as it does not suffer from stagnation.
  Drawbacks: more complex in terms of hardware, as an additional antenna is required. The AUT and the additional antenna have to be connected to the same source/receiver.
- Direct amplitude and phase measurements, also referred to as vector measurements [16]–[18].
  Advantages: very accurate.
  Drawbacks: quite complex in terms of hardware and implementation. Tethered UAV: the UAV and the VNA are connected through an optical fiber cable. Requires very accurate positioning and geo-referring (better than $\lambda/10$). The AUT has to be connected to a VNA concerning phase locking with the probe onboard the UAV.

UAV-based NF antenna measurement systems have to deal with non-uniform acquisition domains. Even though the planned flight path of the UAV could follow a canonical grid (planar, cylindrical, spherical), in practice, there is an offset between the theoretical flight path and the actual one, caused by wind gusts or vibrations of the UAV motors. Thus, processing techniques capable of dealing with non-uniform grids are required. For this purpose, equivalent current-based techniques have been considered for measurements processing. For example, the post-processing conducted in [16]–[18] is based on the fast irregular antenna field transformation algorithm (FIAFTA) [19]. A sources reconstruction method is considered in [9]–[12] (without imposing Love's condition of internal zero field, [20]) and in [13]–[15] (using Love's condition, [21]) for antenna diagnostics and NF-FF transformation.

A summary of the state-of-the-art of the aforementioned UAV-based NF antenna measurement systems is presented in Table 1.

A. AIM AND SCOPE OF THIS CONTRIBUTION

This contribution focuses on the first kind of techniques for UAV-based NF measurements, which is the simplest in terms of hardware, but at the expense of a potential worsening of the accuracy. As mentioned before, the main issue with the iterative phase retrieval technique is the risk of stagnation in local minima. In general, the performance of these iterative methods decreases with the electrical size of the problem (number of measurements and number of unknowns). Recently, it has been proposed the expansion of the equivalent currents using spherical harmonics as an efficient meshless characterization of the currents on the surface enclosing the AUT [23], [24]. The use of meshless basis functions allows working with electrically large antennas while keeping an affordable size of the inverse problem to be solved.

To improve the convergence of the iterative phase retrieval techniques for UAV-based antenna measurements considered in previous contributions [9]–[12], [25], here it is proposed the use of basis functions to reduce the number of unknowns and, consequently, the size of the phaseless retrieval problem.

The rest of the manuscript is structured as follows: Section II revises the phaseless Sources Reconstruction Method (SRM) for amplitude-only field measurements, including the expansion of the equivalent currents using basis functions. Validation with measurements at a spherical range in anechoic chamber is described in Section III, comparing the results obtained without and with basis functions. Results using UAV-based NF measurements of a reflector antenna are presented in Section IV. Finally, Conclusions are drawn in Section V.

II. THE PHASELESS SOURCES RECONSTRUCTION METHOD

A. OVERVIEW OF THE PHASELESS SOURCES RECONSTRUCTION METHOD

The phaseless SRM is an iterative, equivalent currents-based technique that recovers an equivalent electromagnetic model of the AUT from the knowledge of the amplitude of the field radiated by the AUT on two or more surfaces [26]. The underlying idea is the same as those techniques based on the characterization of the AUT using planar modes [27] or spherical modes [28]–[30], with the additional advantage that equivalent current-based methods can work with arbitrary-geometry acquisition and reconstruction domains.

The phaseless SRM for UAV-based NF measurements developed in previous contributions [9]–[12] is a two-stage method, as shown in Fig. 1 flowchart. The first step aims at

TABLE 1. Summary of UAV-based systems capable of NF antenna measurement

Reference and year	Brief description of the system	Antenna(s) used in the validation, and frequency
[9] 2017	Amplitude-only measurements. Monopole antenna probe, two cylindrical measurement surfaces .	2-element array of horn antennas. 2950 MHz and 4650 MHz.
[10] 2018	Amplitude-only measurements. Monopole antenna probe, two semi-cylindrical measurement surfaces.	1800-2300 MHz Base transceiver station (BTS) antenna, working at 2350 MHz. Nominal operation and with partial blockage.
[11] 2019	Amplitude-only measurements. Monopole antenna probe, two surfaces (tested for planar, cylindrical, and semi-cylindrical). Two polarizations.	2-element array of horn antennas, 4650 MHz. 2-element array of helix antennas, 4650 MHz.
[12] 2019	Amplitude-only measurements. Two monopole probes onboard the UAV, planar acquisition domain.	Offset reflector antenna. 4650 MHz.
[13] 2019	Phase retrieval by means of a reference antenna placed close to the AUT. Planar domain, one flight per polarization.	Central element of the Pre Aperture Array Verification System (16 dual-polarized log-periodic elements). 175 MHz.
[16] 2022	Amplitude and phase measurements. Tethered (optical fiber), dual-polarized probe, semi-cylindrical acquisition domain. Optical tracking for accurate positioning.	Horn antenna, 1800 MHz and 2700 MHz.
[17] 2022	Amplitude and phase measurements. Tethered (optical fiber), dual-polarized probe, planar acquisition domain. Laser tracking for accurate positioning.	15-m reflector antenna at 2063 MHz.
[15] 2022	Phase retrieval by means of a reference antenna placed close to the AUT. Planar domain, one flight per polarization.	9.2 m size 16-element array with digital beamforming capabilities (Pre Aperture Array Verification System). 175 MHz.
[22] 2023	Phase retrieval by means of four or more reference antennas placed close to the AUT. Spherical cap of 15 m, zenith drone height of 3 m, scan radius of 8 m. Simulation-based results only.	Simulated 28 $\times$ 20 array antenna at 1 GHz.
[18] 2023	Amplitude and phase measurements, including also a reference antenna. Tethering between the reference antenna and the UAV. Folded-dipole probe, cylindrical sector, single polarization. RTK positioning.	Doppler VHF Omni-directional range (DVOR) antenna, 110 MHz.

retrieving the phase of the acquired field whereas the second one aims at computing the currents from the field retrieved in the previous step.

For this purpose, first, a nonlinear cost function, denoted as C_{NL} (where the subindex NL refers to its non linearity), is minimized. This cost function relates the amplitude of the measured NF at two different surfaces ($|E_{1,2}|$), and the amplitude of the NF radiated by an equivalent currents distribution ($|(Z_{1,2;F})(F)|$), where (F) denotes an equivalent currents distribution and $Z_{1,2;F}$ is the matrix which relates (F) with its radiated NF at the two different surfaces (as derived from the integral equations). Next, these currents are used to estimate the phase of the NF on the measurement surfaces ($\langle\widetilde{E_{1,2}}\rangle$). In the second stage, the complex NF on the acquisition surfaces ($E_{1,2}^{\mathrm{comb}}$) is generated by taking the measured NF amplitude ($|E_{1,2}|$) and the phase estimated in the previous stage ($\langle\widetilde{E_{1,2}}\rangle$). Thus, the amplitude estimated in the previous step is discarded in favor of the one measured. Then, from the complex NF, the SRM [20] is used to reconstruct again an equivalent currents distribution (M_{eq}) that characterizes the AUT [31]. The estimated equivalent current distribution (M_{eq}) is used to calculate the radiation pattern of the AUT.

This two-stage strategy enables the retrieval of the complex equivalent currents from a linear cost function instead of a nonlinear one. This linear cost function is denoted as C_{L}, where the subindex L is used to indicate its linear nature.

The Levenberg-Marquardt algorithm (LMA) [32] was considered in previous contributions to minimize the nonlinear cost function C_{NL} of the first stage. In recent works [28], [33] different algorithms to minimize this kind of nonlinear cost function (e.g. Gerchberg-Saxton, Reweighted Amplitude Flow, Wirtinger flow) have been assessed and compared. Other works have proposed the use of regularization cost functionals to improve the convergence [34]. In the results presented in this contribution, the aforementioned algorithms were tested for the minimization of the nonlinear cost function C_{NL}, finding that LMA and the Reweighted Amplitude Flow provide the best convergence.

B. MINIMIZATION OF THE NUMBER OF EQUIVALENT CURRENTS

One of the main issues affecting the convergence of the algorithms used to minimize the nonlinear cost function C_{NL} is the size of the problem, which is related to the number of measurements and the number of equivalent currents required to characterize the AUT.

Concerning the number of measurements, extensive studies about sampling methods have been described in the literature [35]–[38], being recently introduced for the optimization of the flying path for UAV-based NF measurements [39]. Nevertheless, it must be pointed out that, in the case of UAV-based NF measurements, the effectiveness of these optimal sampling strategies would be conditioned by the

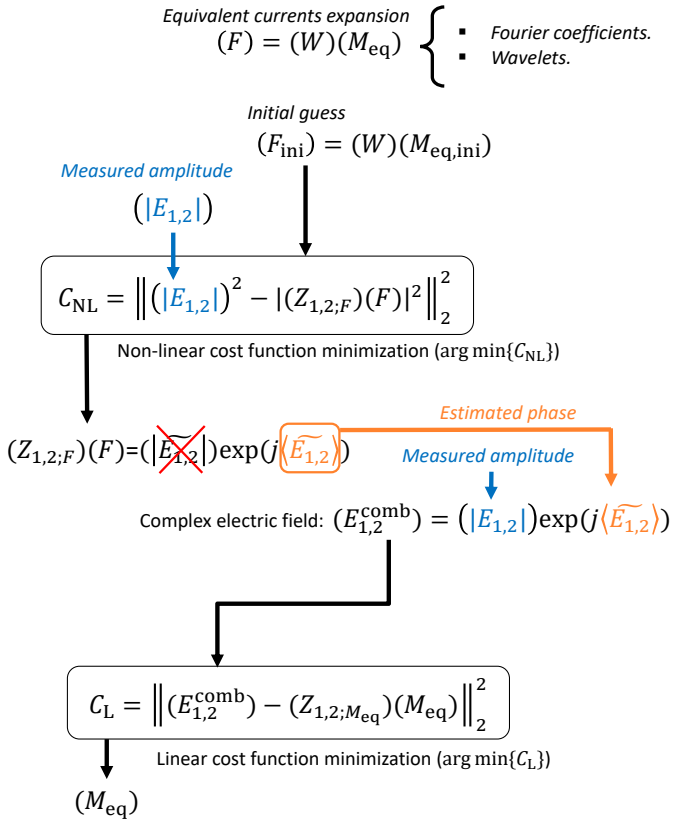

FIGURE 1. Flowchart of the phaseless SRM expanding the equivalent magnetic currents (M_{eq}) with different bases (F). $\|\cdot\|_2$ denotes the L^2 norm (Euclidean norm).

error between the theoretical measurement path and the actual one followed by the UAV.

The number of equivalent currents needed to characterize the AUT is given by the size of the AUT. That is, the equivalent currents are defined in a spatial domain that corresponds to the surface enclosing the AUT, using pulse or Rao-Wilton-Glisson basis functions in most cases.

One possibility to improve the ratio of independent measurements to unknowns and, therefore, the convergence of the phase retrieval method, is related to the use of a single type of equivalent currents. For example, in the case of directive antennas, the application of the Second Electromagnetic Equivalent Principle [31] allows the use of a single set of equivalent currents (magnetic currents) defined on an infinite plane on the AUT aperture plane, which can be truncated to the size of the AUT aperture.

Another possibility is to define a different reconstruction domain where the characterization of the equivalent currents requires fewer basis functions than when the reconstruction is conducted directly in the spatial domain. This idea has been proposed in [23], [24] using spherical harmonics. The calculation of the coefficients (F) characterizing the equivalent currents (M_{eq}) in the transformed, meshless domain, is conducted through the following operation: $(F) = (W)(M_{eq})$, where W is the operator relating both domains. In [38], the authors make use of optimal sampling techniques in both the planar acquisition domain and the reconstruction domain, assuming the AUT to be enclosed by an oblate spheroid. Simulation-based results presented in [38] prove that the reduction of the number of unknowns effectively improves the accuracy of the method.

At this point, it is important to remark that planar, cylindrical, or spherical wave expansion methods for antenna diagnostics and NF-FF transformation are very efficient in terms of the characterization of the AUT and the measured fields using a reduced number of basis functions. However, they require canonical (planar, cylindrical, spherical) domains, while equivalent currents-based techniques are capable of working with arbitrary geometry domains.

The first and simple approach is the use of Fourier coefficients, so that the operator (W) corresponds to the Discrete Fourier Transform (DFT) matrix. If the equivalent currents are reconstructed on the aperture plane of the AUT, the coefficients (F) are related to the Plane Wave Spectrum (PWS) of the field of the AUT on the aperture plane. For this particular case, the FF is obtained directly from the PWS, so the truncation of the coefficients (F) to reduce the number of unknowns will imply a truncation of the valid angular margin of the FF pattern. More precisely, for an aperture sampling rate of $\lambda/2$ (where λ is the wavelength), the PWS is recovered between $-k$ to $+k$ (being k the wavenumber, $k = 2\pi/\lambda$) in both k_x and k_y axes. The relationship between the spectral domain and the FF angular margin (in the θ axis) is given by $\sin(\theta) = k_{max}/k$. Thus, if $k_{max} = \pm k$, $\sin(\theta) = \pm 1$, and thus, the corresponding FF angular margin is the entire visible margin of the PWS, $\theta \in$ [-90° +90°] [40].

To overcome this issue, basis functions that do not limit the FF resolution when truncating the number of coefficients should be considered. In this sense, Discrete Wavelet Transform (DWT) provides both spatial and spectral resolution, thus being a suitable choice for the targeted problem.

III. PERFORMANCE ANALYSIS

A. DESCRIPTION OF THE MEASUREMENT SETUP

This section is devoted to analyze the performance of the phaseless SRM when conducting the expansion of the equivalent currents using Fourier coefficients and wavelets. For this purpose, NF measurements conducted at a spherical range in anechoic chamber are considered. The AUT is an offset reflector antenna fed with a helix antenna. Measurements were conducted at two different distances, R_1 = 3.20 m and R_2 = 5.20 m. Given the working frequency, 4.65 GHz, and the size of the reflector antenna, $D \approx 70$ cm, these distances are within the NF region of the reflector antenna ($R_{FF} = 2D^2/\lambda$ = 11.2 m). The hemi-spherical surfaces were sampled according to Δ_θ = 3°, Δ_ϕ = 6°, with θ = [-60°, 60°]. This results in 1023 measurements per hemi-spherical surface.

NF circular components were composed from the acquisition of linear E_θ and E_ϕ components. For the sake of simplicity, the analysis of the performance of the phaseless SRM is conducted considering just the circular copolar component (right handed component for this antenna, E_{rhc}).

If expressed in terms of the field components, the C_{NL} and C_{L} cost functions become (1) and (2), respectively:

$$C_{\text{NL}} = \left\| \begin{pmatrix} |E_1| \\ |E_2| \end{pmatrix}^2 - \left| \begin{pmatrix} Z_{1;F_x} & Z_{1;F_y} \\ Z_{2;F_x} & Z_{2;F_y} \end{pmatrix} \begin{pmatrix} F_x \\ F_y \end{pmatrix} \right|^2 \right\|_2^2, \quad (1)$$

$$C_{\text{L}} = \left\| \begin{pmatrix} E_1^{\text{comb}} \\ E_2^{\text{comb}} \end{pmatrix} - \begin{pmatrix} Z_{1;M_x} & Z_{1;M_y} \\ Z_{2;M_x} & Z_{2;M_y} \end{pmatrix} \begin{pmatrix} M_x \\ M_y \end{pmatrix} \right\|_2^2, \quad (2)$$

where $\|\cdot\|$ denotes the L^2 norm. $|E_1|$, $|E_2|$ are the measured components of the NF amplitude at two different surfaces (in this case, the right handed circular polarization, E_{rhc}); F_x, F_y denotes an equivalent magnetic current distribution expanded considering a given basis (with the subindexes x and y referring to the x and y components of the magnetic currents); and the submatrixes $Z_{i;F_t}$ ($i = \{1, 2\}$ and $t = \{x, y\}$) relate F_t with its corresponding NF component at the $i-$th surface. E_1^{comb} and E_2^{comb} are the estimated complex NF (using the estimated phase and the measured amplitude) at the two acquisition surfaces; M_x, M_y are the x and y components of the equivalent magnetic currents distribution characterizing the antenna; and the submatrixes $Z_{i;M_t}$ ($i = \{1, 2\}$ and $t = \{x, y\}$) relate M_t with its corresponding NF component at the $i-$th surface.

A picture of the reflector antenna being measured at the spherical range in anechoic chamber of the University of Oviedo is depicted in Fig. 2. The amplitude of the right handed component at the distances of R_1 = 3.20 m and R_2 = 5.20 m is plotted in Fig. 3.

B. ANTENNA DIAGNOSTICS AND NF-FF TRANSFORMATION RESULTS

From the amplitude of the NF measured at the two hemispherical acquisition surfaces, the cost function C_{NL} is minimized to retrieve the coefficients (F) and, from these, estimate the phase corresponding to the measured NF amplitude. Fourier and wavelet coefficients (more precisely, Daubechies orthogonal wavelets of level 4 (*db4*) [41]), were considered in this example.

The offset reflector is a directive antenna, so it can be characterized by defining an equivalent magnetic currents distribution on its aperture. For this antenna, the truncated aperture plane had a size of x = 110 cm $\times$ y = 110 cm, discretized every 0.55λ in both directions. This results in 2046 unknowns, since the circular polarization is expressed as the combination of two linear components. It should be clarified that the basis functions in the spatial domain for SRM are pulses (of $0.55\lambda \times 0.55\lambda$), and the coefficients of the Fourier and wavelet transforms are defined for this set of spatial basis functions. According to [42], FF pattern aliasing

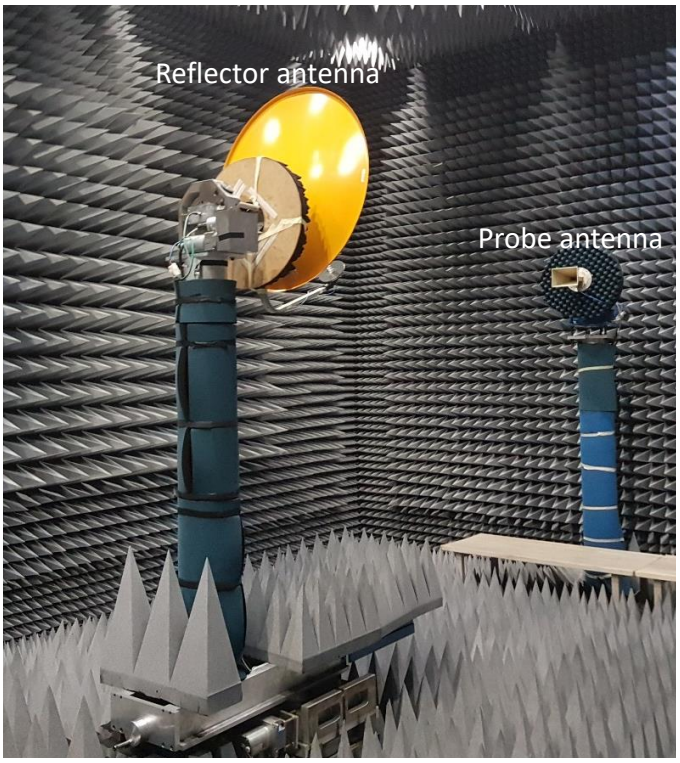

FIGURE 2. Picture of the offset reflector antenna being measured at the spherical range in anechoic chamber of the University of Oviedo.

caused by the choice of basis functions slightly larger than half a wavelength is negligible for directive antennas.

The analysis of the convergence of the minimization of the cost function C_{NL} is plotted in Fig. 4. For comparison purposes, 100 iterations are represented, and the metric is defined as $|||E_{1,2}| - |(Z_{1,2;F})(F)|||_2^2 / ||E_{1,2}||_2^2$. When the coefficients (F) are defined in the spatial domain (red line in Fig. 4), the method stagnates after 60 iterations.

Once the phase of the NF is recovered, the SRM is applied to reconstruct again the equivalent currents on the aperture plane of the AUT, but this time using the complex NF constructed from the measured amplitude and the recovered phase. The amplitude of these currents (which, in turn, are the electric field on the aperture plane) is plotted in the left column of Fig. 5. In particular, Fig. 5 (b) corresponds to the results when the coefficients (F) are defined in the spatial domain (that is, the aperture plane of the AUT). For reference purposes, the equivalent magnetic currents reconstructed from complex NF measurements at the anechoic chamber are shown in Fig. 5 (a).

Next, Fourier and wavelet coefficients are introduced. In the case of wavelet coefficients, the truncation threshold corresponds to the percentage of the coefficients with highest amplitudes. Truncation of Fourier coefficients is conducted on the k_x, k_y domain by defining a rectangular region that also contains the highest amplitude coefficients. In the examples presented in this contribution, the percentage of Fourier or wavelet coefficients denotes the number of coefficients

This article has been accepted for publication in IEEE Open Journal of Antennas and Propagation. This is the author's version which has not been fully edited and content may change prior to final publication. Citation information: DOI 10.1109/OJAP.2024.3393432

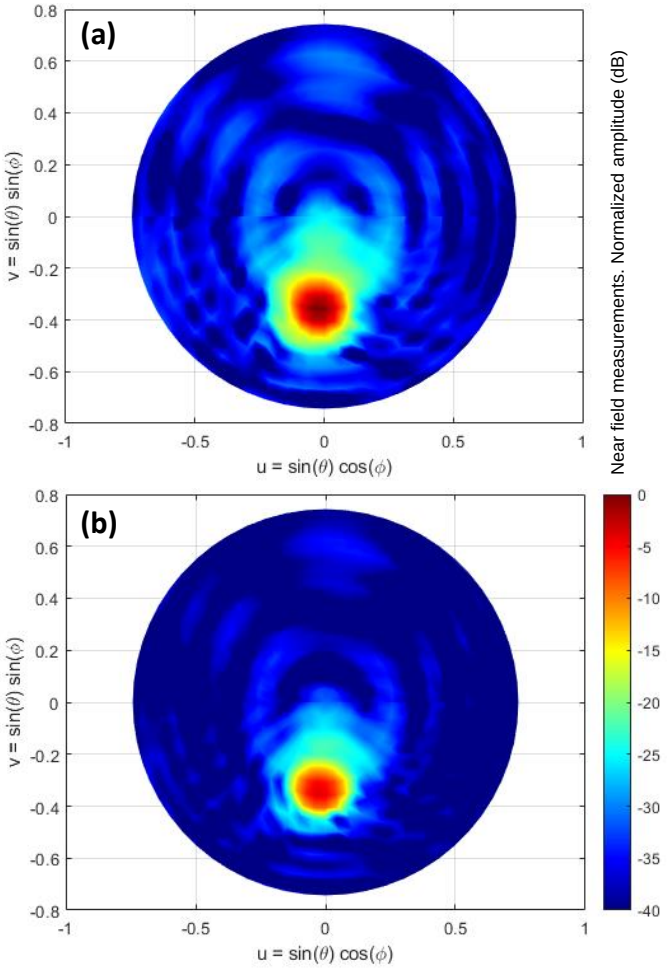

FIGURE 3. **Amplitude of the right handed circular component measured at the NF distances of (a) R_1 = 3.20 m and (b) R_2 = 5.20 m.**

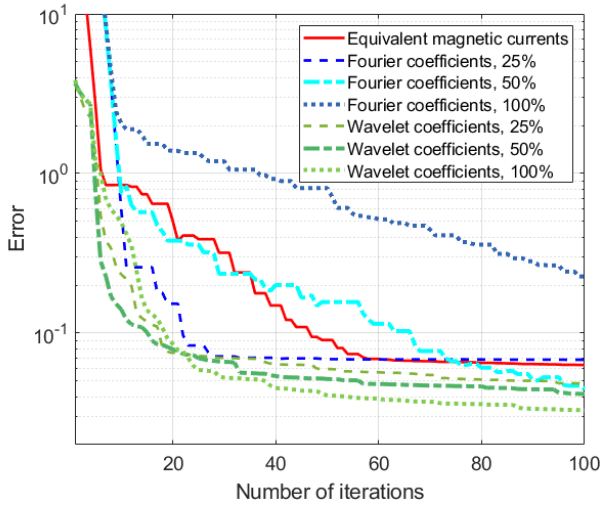

FIGURE 4. **Comparison of the convergence of the different cases listed in Table 2. Error =** $|||E_{1,2}| - |(Z_{1,2;F})(F)|||_2^2/||E_{1,2}||_2^2$.

TABLE 2. **Analysis of the convergence and computational cost of the phaseless SRM. Phaseless measurements at a spherical range in anechoic chamber.**

Method	Number of unknowns (M)	Condition number of ($Z_{1,2;F}$) matrix	Calculation time for 100 iterations
Spatial domain (equivalent currents)	2046	$5.2807{\cdot}10^{21}$	999 s
Fourier, 25 % coefficients	512	$1.2808{\cdot}10^{5}$	19 s
Fourier, 50 % coefficients	1023	$2.7848{\cdot}10^{7}$	179 s
Fourier, 100 % coefficients	2046	$9.0838{\cdot}10^{16}$	929 s
Wavelets, 25 % coefficients	512	$7.4656{\cdot}10^{4}$	16 s
Wavelets, 50 % coefficients	1023	$1.7933{\cdot}10^{6}$	168 s
Wavelets, 100 % coefficients	2046	$6.0312{\cdot}10^{21}$	937 s

Number of equations (measurements) (N) is 2046 for all the cases.

kept with respect to the overall number of coefficients. In particular, results when keeping 25 %, 50 %, and 100 % of the coefficients, will be considered.

From the explanation given in the previous paragraph, it can be inferred that truncation of the coefficients requires solving first the problem with all the unknowns. To overcome this issue, the problem is solved first for an initial guess using pulse basis functions. The corresponding Fourier and wavelet coefficients are calculated from that initial solution and, after sorting the coefficients by amplitude, those beyond a given percentage or a given threshold are discarded. The corresponding transform matrix is built only for those coefficients. This initial guess can be set based on a-priori information of the AUT (e.g., it might consist of a uniform distribution of equivalent magnetic currents fitting the aperture of the AUT).

For each analyzed configuration involving equivalent currents, Fourier coefficients, and wavelet coefficients, the number of unknowns is given in Table 2, together with the calculation time required for 100 iterations of the cost function minimization algorithm (coded in Matlab^{TM}, and run on a conventional laptop with 16 GB RAM and 6-core Intel Core i7 processor).

From the analysis of the error depicted in Fig. 4, it is concluded that reducing the number of coefficients and, consequently, the number of unknowns, improves the convergence of the phase retrieval algorithm. This is especially noticeable for Fourier coefficients (blue lines in Fig. 4). Wavelet coefficients (green lines in Fig. 4) provide the best convergence and the lowest error. The 2-norm condition number of the $(Z_{1,2;F})$ matrix is shown in the third column

of Table 2, proving that the reduction of the unknowns, and thus the reduction of the size of the matrix, improves the conditioning of the matrix.

Reconstructed equivalent currents using Fourier and wavelet coefficients are represented in Fig. 5 (c)-(e) (left column), and in Fig. 6 (left column), respectively. The use of wavelet coefficients results in an equivalent currents distribution closer to the ones obtained from complex measurements (Fig. 5 (a)) than those recovered with Fourier coefficients.

From the reconstructed equivalent currents on the aperture plane, the FF of the reflector antenna is computed. The accuracy of the recovery of the FF from NF measurements is one key performance indicator when assessing NF antenna measurement systems. The 2D u-v representation of the FF is provided in the right columns of Fig. 5 and Fig. 6, and the cuts of the FF pattern are plotted in Fig. 7. From the comparison of Fig. 7 (a) and Fig. 7 (b), it is concluded that the number of Fourier and wavelet coefficients has little impact in the results. Only when wavelet coefficients were used, the FF pattern closely matches the reference one obtained from complex NF measurements. In particular, the closest agreement was achieved when 25 % of wavelet coefficients were kept (Fig. 7 (b) and (c)). Also, the result is less sensitive to the variation in the number of coefficients.

For a better comparison, the Equivalent Stray Signal (ESS) between the reference pattern and those ones depicted in Fig. 7 (c) has been calculated and plotted in Fig. 8. The definition of the ESS is provided in (3) [43],

$$\begin{aligned} \mathrm{ESS(dB)} &= E_{\mathrm{est}}(\mathrm{dB}) + 20\log_{10}\left(\frac{1-10^{-\Delta/20}}{2}\right), \\ \Delta &= E_{\mathrm{est}}(\mathrm{dB}) - E_{\mathrm{ref}}(\mathrm{dB}), \end{aligned} \tag{3}$$

where $E_{\mathrm{ref}}(\mathrm{dB})$ is the reference pattern and $E_{\mathrm{est}}(\mathrm{dB})$ is the pattern to be compared with the reference one.

The maximum ESS using 25 % of wavelet coefficients (Fig. 8, green dotted line) is almost 10 dB lower than the ESS associated with Fourier coefficients (Fig. 8, blue dashed line) or the equivalent currents defined in the spatial domain (Fig. 8, red dashed line).

A parametric analysis of the ESS as a function of the number of Fourier and wavelet coefficients has been conducted, whose results are shown in Fig. 9. It can be noticed that the use of wavelet coefficients results in a lower ESS than in the case of Fourier coefficients, with the optimum number of coefficients between 15 % and 35 %. In the case of Fourier coefficients, lower values of ESS are obtained for percentages between 45 % and 70 %.

The main conclusions that can be drawn from the analysis carried out in this section are:

i) The use of wavelet coefficients allows recovering the FF pattern using 75 % fewer unknowns than those required if defining the equivalent currents in the spatial domain. This result is supported by the analysis of the convergence of the minimization of the nonlinear cost function C_{NL} and the condition number of the matrix $(Z_{1,2;F})$.

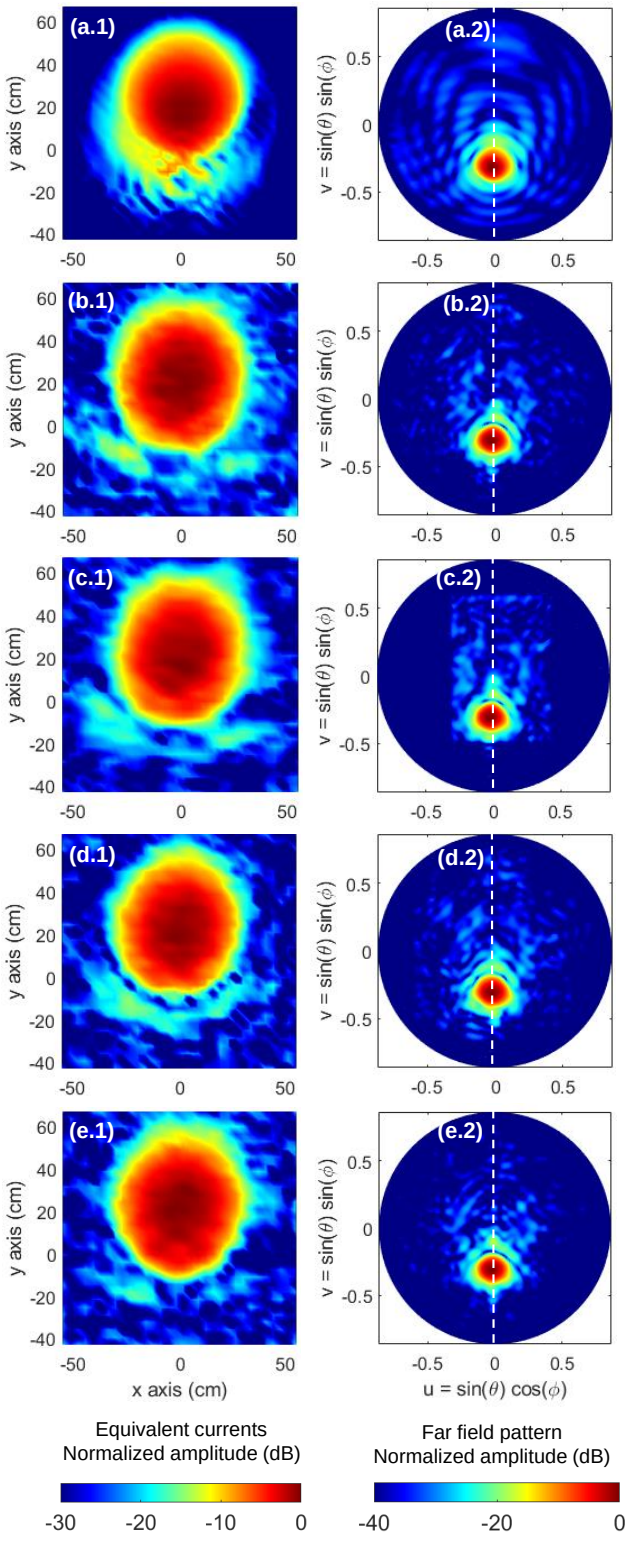

FIGURE 5. Reconstructed equivalent currents, right handed circular component (left column) and the corresponding radiation pattern (right column) of the offset reflector antenna. (a) From amplitude and phase measurements. (b) From amplitude-only measurements, phaseless SRM. (c) From amplitude-only measurements, phaseless SRM, 25 % of Fourier coefficients. (d) From amplitude-only measurements, phaseless SRM, 50 % of Fourier coefficients. (e) From amplitude-only measurements, phaseless SRM, 100 % of Fourier coefficients. The white dashed line denotes the ϕ = 90° cut of the pattern.

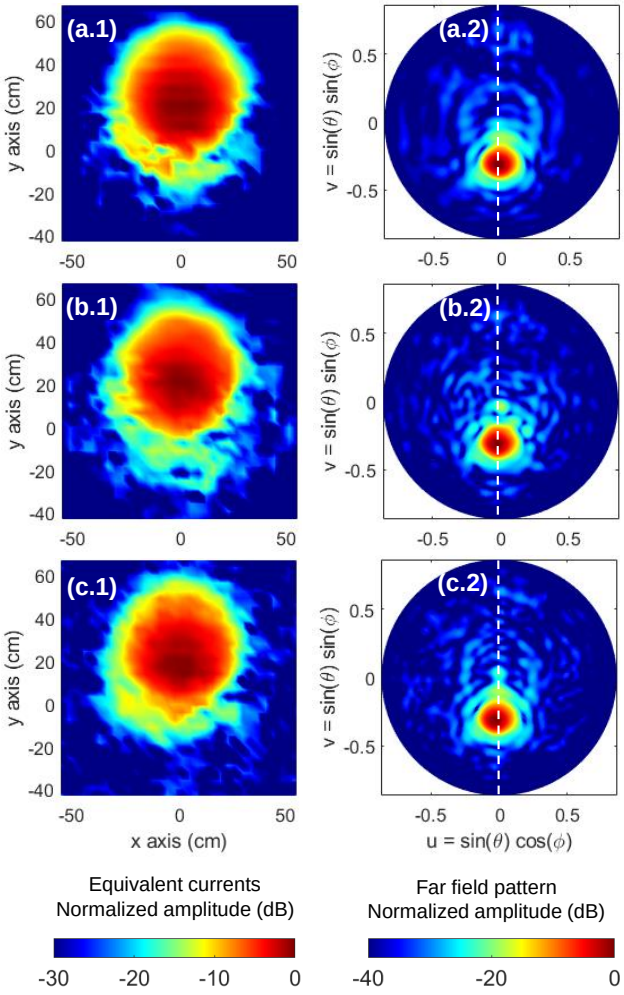

FIGURE 6. **Reconstructed equivalent currents, right handed circular component (left column) and the corresponding radiation pattern (right column) of the offset reflector antenna. (a) From amplitude-only measurements, phaseless SRM, 25 % of wavelet coefficients. (b) From amplitude-only measurements, phaseless SRM, 50 % of wavelet coefficients. (c) From amplitude-only measurements, phaseless SRM, 100 % of wavelet coefficients. The white dashed line denotes the $\phi = 90^\circ$ cut of the pattern.**

ii) Fourier coefficients truncated to 25 % show a similar convergence of the nonlinear cost function C_{NL} than wavelets, but the FF pattern is not accurately predicted with the former coefficients. The explanation is that, as pointed out in Section B, these Fourier coefficients are related to the PWS of the aperture field and, hence, to the FF pattern. That means that truncating the Fourier coefficients implies truncating the valid angular margin of the FF pattern. This can be better observed in Fig. 5 (c.2), which corresponds to the FF considering 25 % of the Fourier coefficients. The valid angular margin of the FF pattern is recovered in just part of the u-v domain (i.e. those angular values associated with non-zero Fourier coefficients). As a result, the choice of the number of Fourier coefficients involves a trade-off between the reduction of the number of unknowns and the

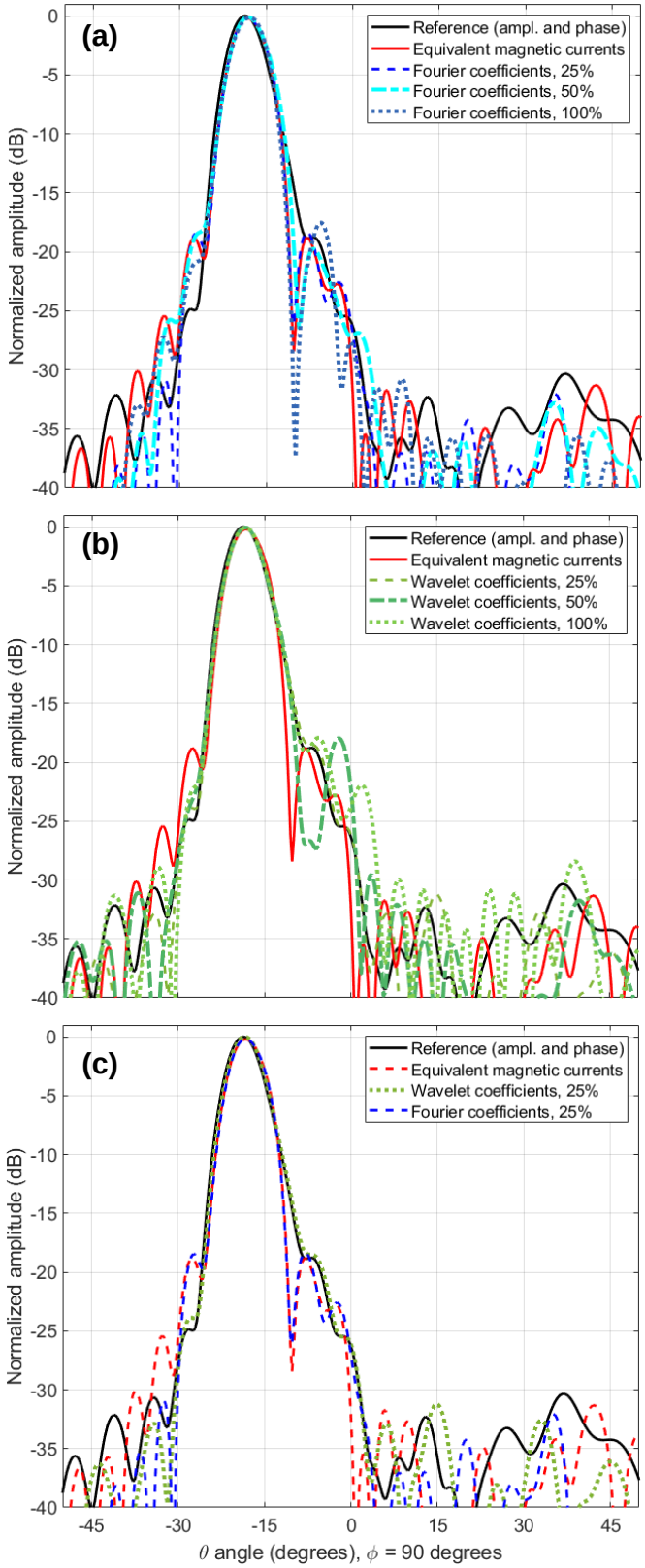

FIGURE 7. **Comparison of the radiation patterns ($\phi = 90^\circ$ cut) calculated from the reconstructed equivalent currents depicted in Fig. 5 and Fig. 6.**

This article has been accepted for publication in IEEE Open Journal of Antennas and Propagation. This is the author's version which has not been fully edited and content may change prior to final publication. Citation information: DOI 10.1109/OJAP.2024.3393432

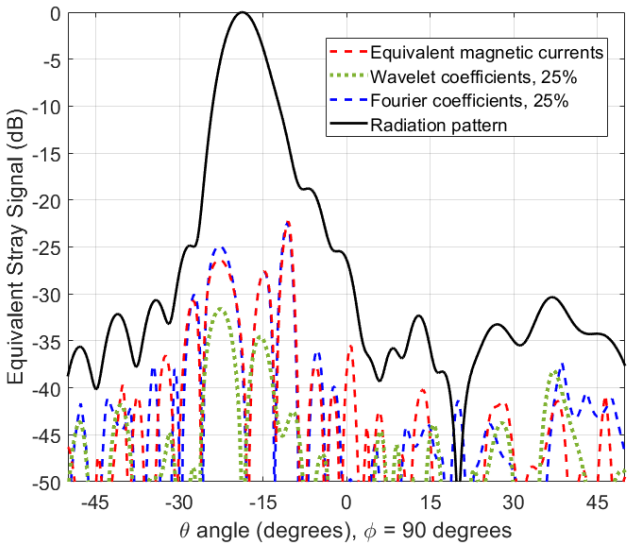

FIGURE 8. **Equivalent Stray Signal (ESS) between the reference radiation pattern (black line) and the ones depicted in Fig. 7 (c).**

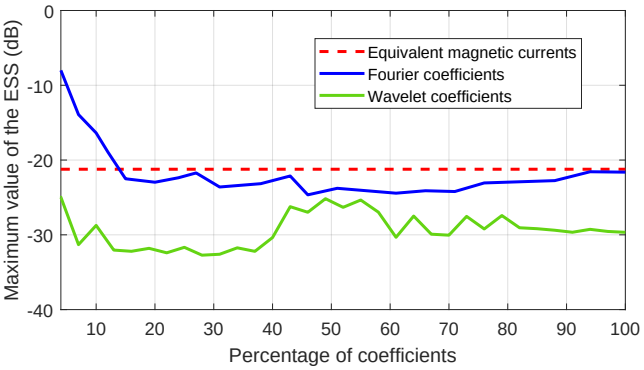

FIGURE 9. **Maximum value of the ESS as a function of the number of Fourier and wavelet coefficients. ESS when equivalent magnetic currents are considered is depicted for comparison purposes.**

extension of the valid angular margin of the FF pattern which in turn affects the convergence and, as observed in Fig. 9, the error (ESS).

Finally, the calculation time associated with the phaseless SRM for this example is shown in the fourth column of Table 2. For every LMA iteration, the inversion of a square matrix of size $M \times M$ is required. Thus, the calculation time of the LMA is greatly affected by the number of unknowns (M) rather than the number of equations (N). This can be observed when comparing the calculation time for the different number of coefficients considered. The use of other iterative phase retrieval methods, e.g. Reweighted Amplitude Flow [44], exhibits similar behavior in terms of computational complexity.

IV. UAV-BASED MEASUREMENTS

In this section, the phaseless SRM using basis functions to expand the equivalent currents is tested with amplitude-only measurements collected using a UAV-based antenna measurement system. One of the main features and novelties of the system is the capability to acquire the amplitude of the radiated field simultaneously at the two measurement surfaces [25], thus minimizing uncertainties and positioning errors compared to those systems where two independent flights are needed to acquire the tangential electric field on each surface.

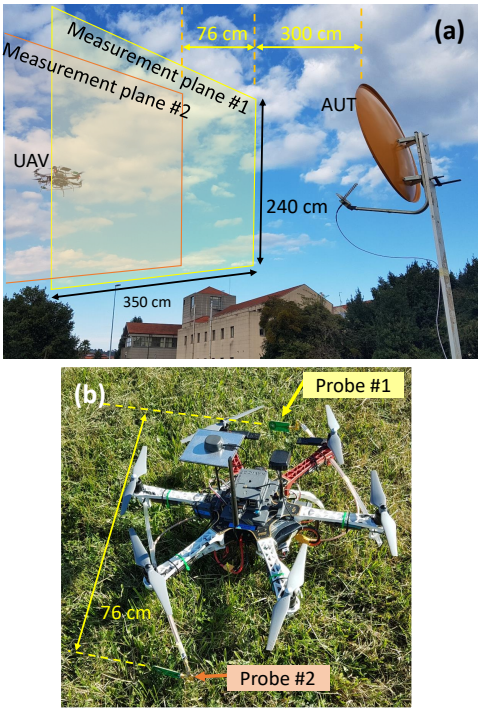

FIGURE 10. **(a) Picture of the UAV-based antenna measurement setup, indicating the size of the acquisition surfaces and the distance to the AUT (offset reflector antenna). (b) Picture of the two-probe UAV-based antenna measurement system [25].**

To achieve this, the radiofrequency detector onboard the UAV has two input channels that are connected to two dipole-like probe antennas placed as separated as possible (76 cm in this prototype), as depicted in Fig. 10. This configuration enables simultaneous measurements of the electric field radiated by the AUT in two identical surfaces but 76 cm separated each other. A detailed description of the implemented dual-probe antenna measurement system prototype can be found in [12].

The same 70 cm diameter offset reflector antenna as in Section III was considered, working at the same frequency of 4.65 GHz. This is a directive antenna, so a planar acquisition domain was considered as a trade-off between measurement setup complexity and truncation of the valid angular margin of the FF pattern [45]. The choice of the size of the NF measurement planes and the distance to the AUT was discussed in [12], together with the results of a parametric study of the phaseless SRM convergence as a function of this distance between the AUT and the measurement planes.

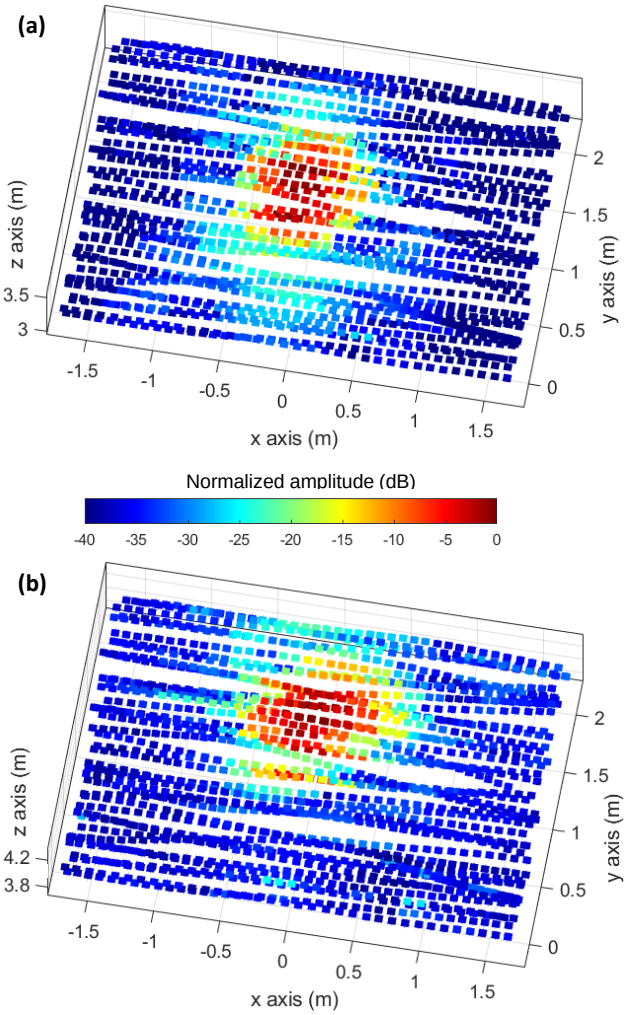

FIGURE 11. Representation of the NF amplitude of the electric field ($|E_x|$ component) acquired using the two-probe UAV-based antenna measurement system. (a) Plane 1 (placed 3 m away from the AUT). (b) Plane 2 (placed 3.76 m away).

The amplitude of the measured NF at the geo-referred acquisition points is plotted in Fig. 11. The approximate size of the acquisition planes is 3.5 m width × 2.4 m height. 6607 NF samples were acquired on each plane (∼ 97 × 68), resulting in a sampling rate of $\sim \lambda/2$. Given the sizes of the measurement planes, their distance to the AUT, and the AUT size, the valid angular margin of the FF pattern is calculated as indicated in Section 5.3.1.6 of [45], resulting in a margin of ± 15° in the vertical plane. The acquisition planes are approximately centered at the position of the maximum of the radiated field (Fig.11), so the main lobe is located approximately at the center of the ± 15° angular margin.

As observed in Fig. 10 (b), the dipole-like probe antennas have horizontal polarization (x axis given the axis definition). Although the full characterization of the NF radiated by the AUT would require measuring both linear or circular components, in this example only the E_x component of the field radiated by the reflector antenna will be considered for validation purposes. Consequently, the C_{NL} and C_{L} cost functions become (4,5):

$$C_{\mathrm{NL}} = \left\| \begin{pmatrix} |E_{x1}| \\ |E_{x2}| \end{pmatrix}^2 - \left| \begin{pmatrix} Z_{1;F_y} \\ Z_{2;F_y} \end{pmatrix} \begin{pmatrix} F_y \end{pmatrix} \right|^2 \right\|_2^2, \quad (4)$$

$$C_{\mathrm{L}} = \left\| \begin{pmatrix} E_{x1}^{\mathrm{comb}} \\ E_{x2}^{\mathrm{comb}} \end{pmatrix} - \begin{pmatrix} Z_{1;M_y} \\ Z_{2;M_y} \end{pmatrix} \begin{pmatrix} M_y \end{pmatrix} \right\|_2^2. \quad (5)$$

The geo-referred NF measurements are first used to recover the phase of the NF, then the equivalent magnetic currents on the AUT aperture plane, and finally, the FF pattern. For comparison purposes, the measurements of Section III, conducted at a spherical range in anechoic chamber, were processed again but considering just the E_x component of the measured NF (that is, the NF-FF transformation will be conducted using just the E_x component). The truncated aperture plane of the AUT has a size of x = 100 cm × y = 100 cm, and it is discretized every $\lambda/2$ (i.e. 1024 mesh elements). The use of planar domains allows decoupling the integral equations relating fields and equivalent currents [46], thus enabling recovering M_y from E_x.

A summary of the problem size, condition number of the problem, and calculation time is compiled in Table 3. As in the example of Section III, the use of wavelet basis functions improves the conditioning thanks to the lower number of unknowns.

The convergence of the minimization of the cost function C_{NL} is also compared in Fig. 12. First, it can be observed that anechoic chamber measurements of the E_x component exhibit better convergence than UAV-based measurements.

TABLE 3. Analysis of the convergence and computational cost of the phaseless SRM when acquiring E_x. Anechoic chamber and UAV-based NF measurements.

Method	Number of unknowns (M)	Condition number of ($Z_{1,2;F}$) matrix	Calculation time for 100 iterations
Anechoic chamber meas., spatial domain (equivalent currents)	1023	$3.2978{\cdot}10^{14}$	136 s
Anechoic chamber meas., wavelets, 25 % coefficients	256	$9.97{\cdot}10^{2}$	8 s
UAV, spatial domain (equivalent currents)	1024	$1.6326{\cdot}10^{14}$	160 s
UAV meas., wavelets, 25 % coefficients	256	$5.8022{\cdot}10^{6}$	11 s
UAV meas., wavelets, 50 % coefficients	512	$3.1562{\cdot}10^{13}$	28 s
UAV meas., wavelets, 100 % coefficients	1024	$1.62917{\cdot}10^{14}$	165 s

Anechoic chamber: number of measurements (N) is 2046.
UAV-based acquisition: number of measurements (N) is 13124.

This article has been accepted for publication in IEEE Open Journal of Antennas and Propagation. This is the author's version which has not been fully edited and content may change prior to final publication. Citation information: DOI 10.1109/OJAP.2024.3393432

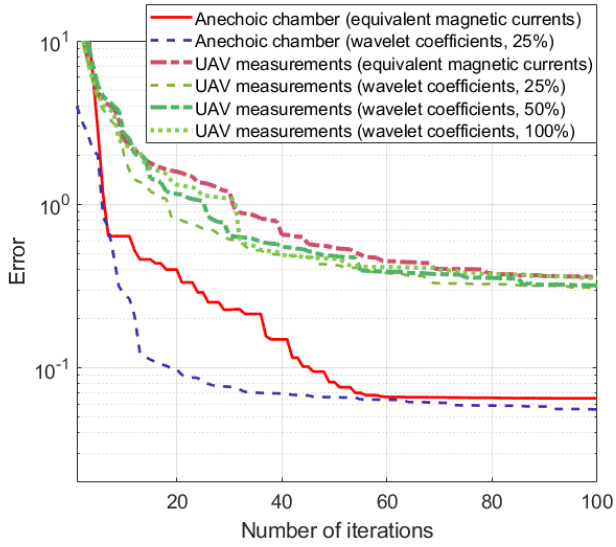

FIGURE 12. **Convergence of the different cases listed in Table 3.**

This is due to the higher degree of accuracy in terms of dynamic range, noise, and positioning of the former. When comparing those results corresponding to coefficients F defined in the spatial domain and using wavelets, the latter shows faster convergence (again, this improvement is more noticeable for anechoic chamber measurements).

The reconstructed equivalent currents (M_y component) on the reflector aperture plane and the corresponding FF pattern are depicted in Fig. 13. In the case of anechoic chamber measurements, the best agreement between amplitude and phase results (Fig. 13 (a)) and amplitude-only ones is achieved for the case of 25 % of wavelet coefficients (Fig. 13 (c)). This result is supported by the FF pattern comparison plotted in Fig. 14 (a), where the difference between the FF pattern from amplitude and phase measurements (black line) and the FF pattern obtained from 25 % of wavelet coefficients (blue dashed line) is less than 1 dB within the $\pm$ 15° FF valid angular margin.

The FF pattern recovered from amplitude-only measurements collected with the UAV-based antenna measurement system is depicted in Fig. 13 (d.2) and in Fig. 14 (b). Despite the inherent uncertainties of the UAV system and the truncated planar acquisition domain, it is observed that, again, the best results are achieved when considering 25 % of wavelet coefficients (dashed green line). It should be noted that results for other percentages of wavelet coefficients were also analyzed, finding that the aperture fields and the corresponding FF pattern were not accurately retrieved when less than 20 % wavelet coefficients were considered. Thus, for this example, the optimum number of wavelet coefficients is around 20 % - 30 %.

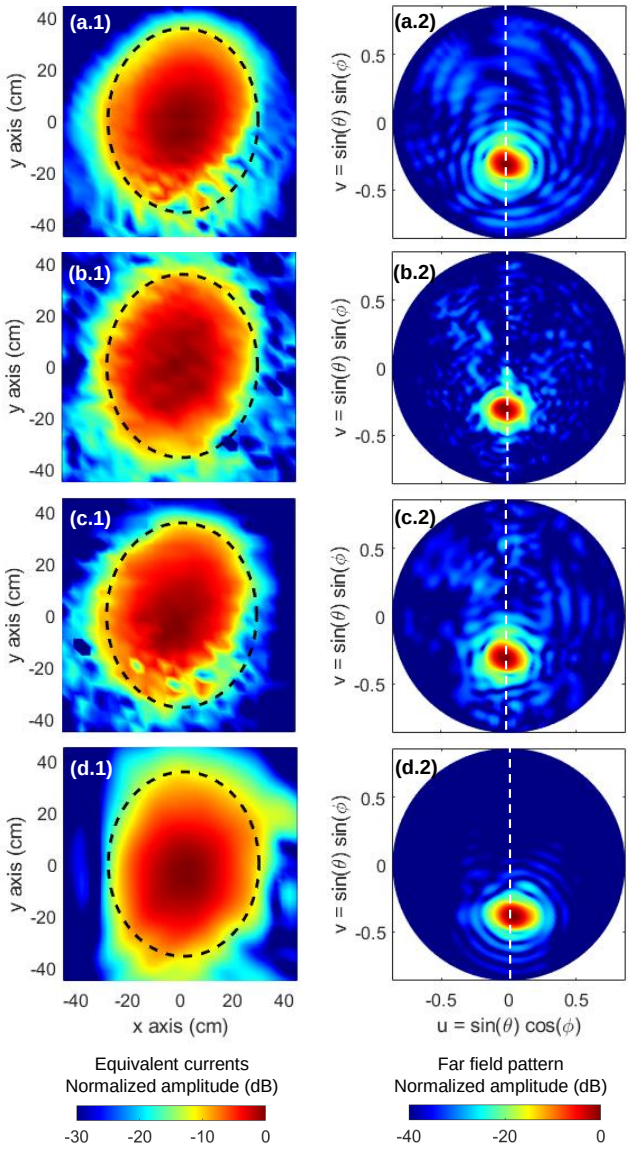

FIGURE 13. **Reconstructed equivalent currents, M_y component (left column) and the associated radiation pattern (right column). (a-c) Measurement of the E_x component of the offset reflector antenna at a spherical range in anechoic chamber. (a) From amplitude and phase NF measurements. (b) From amplitude-only measurements, phaseless SRM. (c) From amplitude-only measurements, phaseless SRM, 25 % of wavelet coefficients. (d) Measurement of the E_x component of the offset reflector antenna using the UAV-based two-probe antenna measurement system, phaseless SRM, 25 % of wavelet coefficients. The dashed black ellipse represents the size of the offset reflector antenna, and the white dashed line denotes the ϕ = 90 ° cut of the pattern.**

V. CONCLUSION

This manuscript has presented a method to improve the performance of a phaseless SRM concerning its application

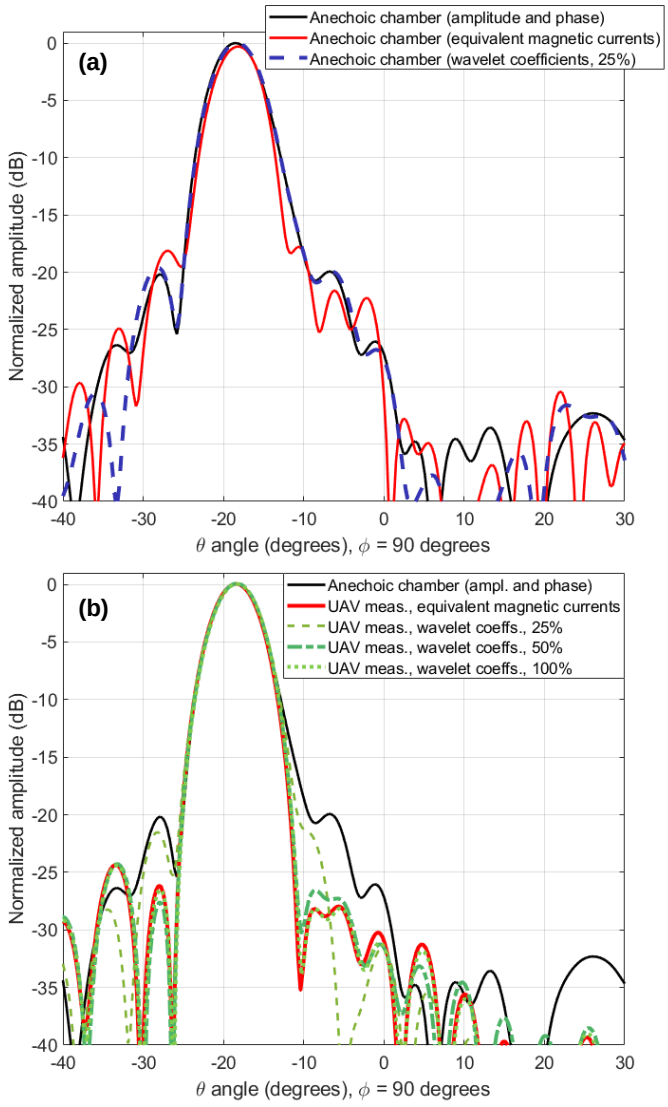

FIGURE 14. Comparison of the radiation patterns (ϕ = 90° cut) calculated from the equivalent currents. (a) Reconstructed from anechoic chamber measurements. (b) Reconstructed from amplitude-only UAV-based measurements.

to amplitude-only UAV-based antenna measurement systems. Different kinds of basis functions to expand the equivalent currents from a spatial domain to a meshless one were tested, aiming at reducing the number of unknowns needed to characterize these equivalent currents. Fourier coefficients were tested, finding that they are not a suitable option as their truncation also affects the extension of the FF angular margin. To overcome this issue, wavelet coefficients were assessed, finding that they effectively improve the convergence of the phaseless SRM, while having little or no impact on the FF angular margin. Results presented in this contribution prove that the reduction in the number of unknowns needed to characterize the AUT successfully improves the accuracy of the phaseless SRM. More precisely, it was found that around 25 % of wavelet coefficients (which, in turn, corresponds also to 25 % of the equivalent currents defined in the spatial domain) are sufficient to accurately characterize the reflector antenna considered in the examples.

REFERENCES

[1] A. Y. Umeyama, J. L. Salazar-Cerreno, and C. J. Fulton, "UAV-based far-field antenna pattern measurement method for polarimetric weather radars: Simulation and error analysis," *IEEE Access*, vol. 8, pp. 191 124–191 137, 2020.

[2] G. Virone, S. Matteoli, F. Paonessa, P. Bolli, S. J. Wijnholds, L. Ciorba, G. Addamo, and O. A. Peverini, "Preliminary results on the verification of the lofar-hba with a flying test source," in *2021 15th European Conference on Antennas and Propagation (EuCAP)*, 2021, pp. 1–4.

[3] A. Salari and D. Erricolo, "Unmanned aerial vehicles for high-frequency measurements: An accurate, fast, and cost-effective technology," *IEEE Antennas and Propagation Magazine*, vol. 64, no. 1, pp. 39–49, 2022.

[4] C. Culotta-López, S. Skeidsvoll, A. Buchi, and J. Espeland, "Use of UASs for outdoor diagnostics of large antennas," in *2022 Antenna Measurement Techniques Association Symposium (AMTA)*, 2022, pp. 1–4.

[5] G. Virone, A. M. Lingua, M. Piras, A. Cina, F. Perini, J. Monari, F. Paonessa, O. A. Peverini, G. Addamo, and R. Tascone, "Antenna pattern verification system based on a micro unmanned aerial vehicle (UAV)," *IEEE Antennas and Wireless Propagation Letters*, vol. 13, pp. 169–172, 2014.

[6] C. Chang, C. Monstein, A. Refregier, A. Amara, A. Glauser, and S. Casura, "Beam calibration of radio telescopes with drones," in *Publications of the Astronomical Society of the Pacific*, vol. 127, 2015, pp. 1131–1143.

[7] J. Schreiber, "Antenna pattern reconstitution using unmanned aerial vehicles (UAVs)," in *IEEE Conference on Antenna Measurements and Applications (CAMA)*, 2016, pp. 1–3.

[8] T. Fritzel, R. Strauß, H.-J. Steiner, C. Eisner, and T. Eibert, "Introduction into an UAV-based near-field system for in-situ and large-scale antenna measurements (invited paper)," in *2016 IEEE Conference on Antenna Measurements and Applications (CAMA)*, 2016, pp. 1–3.

[9] M. García-Fernández, Y. Álvarez López, A. Arboleya, B. González-Valdés, Y. Rodríguez-Vaqueiro, M. E. De Cos Gómez, and F. Las-Heras Andrés, "Antenna diagnostics and characterization using unmanned aerial vehicles," *IEEE Access*, vol. 5, pp. 23 563–23 575, 2017.

[10] M. G. Fernandez, Y. A. Lopez, and F. L.-H. Andres, "On the use of unmanned aerial vehicles for antenna and coverage diagnostics in mobile networks," *IEEE Communications Magazine*, vol. 56, no. 7, pp. 72–78, 2018.

[11] M. Garcia-Fernandez, Y. A. Lopez, and F. L.-H. Andres, "Unmanned aerial system for antenna measurement and diagnosis: evaluation and testing," *IET Microwaves, Antennas & Propagation*, vol. 13, no. 13, pp. 2224–2231, 2019. [Online]. Available: https://ietresearch.onlinelibrary.wiley.com/doi/abs/10.1049/iet-map.2018.6167

[12] M. García Fernández, Y. Álvarez López, and F. Las-Heras, "Dual-probe near-field phaseless antenna measurement system on board a UAV," *Sensors*, vol. 19, no. 21, 2019. [Online]. Available: https://www.mdpi.com/1424-8220/19/21/4663

[13] L. Ciorba, G. Virone, F. Paonessa, S. Matteoli, P. Bolli, E. de Lera Acedo, N. Razavi Ghods, J. Abraham, E. C. Beltrán, K. Zarb Adami, A. Magro, O. A. Peverini, G. Addamo, G. Giordanengo, M. Righero, and G. Vecchi, "Near-field phase reconstruction for UAV-based antenna measurements," in *2019 13th European Conference on Antennas and Propagation (EuCAP)*, 2019, pp. 1–4.

[14] ——, "Near-field phase reconstruction for UAV-based antenna measurements," in *2019 13th European Conference on Antennas and Propagation (EuCAP)*, 2019, pp. 1–4.

[15] L. Ciorba, G. Virone, F. Paonessa, M. Righero, E. De Lera Acedo, S. Matteoli, E. C. Beltran, P. Bolli, G. Giordanengo, G. Vecchi, A. Magro, R. Chiello, O. A. Peverini, and G. Addamo, "Large horizontal near-field scanner based on a non-tethered unmanned aerial vehicle," *IEEE Open Journal of Antennas and Propagation*, vol. 3, pp. 568–582, 2022.

[16] R. A. M. Mauermayer and J. Kornprobst, "A cost-effective tethered-UAV-based coherent near-field antenna measurement system," *IEEE*

Open Journal of Antennas and Propagation, vol. 3, pp. 984–1002, 2022.

[17] S. Punzet, F. T. Faul, T. Mittereder, C. Oettl, M. Ganser, M. Häusler, and T. F. Eibert, "Fully coherent UAV-based near-field measurement and transformation of the s67-15 m ground station antenna at the german space operations center in weilheim," in *2022 16th European Conference on Antennas and Propagation (EuCAP)*, 2022, pp. 1–5.

[18] T. F. Eibert, S. Punzet, T. Mittereder, F. T. Faul, and A. H. Paulus, "UAV-based near-field measurements at a doppler very high frequency omnidirectional radio range," in *2023 17th European Conference on Antennas and Propagation (EuCAP)*, 2023, pp. 1–5.

[19] O. Neitz, R. A. M. Mauermayer, Y. Weitsch, and T. F. Eibert, "A propagating plane-wave-based near-field transmission equation for antenna gain determination from irregular measurement samples," *IEEE Transactions on Antennas and Propagation*, vol. 65, no. 8, pp. 4230–4238, 2017.

[20] Y. Alvarez, F. Las-Heras, and M. R. Pino, "Reconstruction of equivalent currents distribution over arbitrary three-dimensional surfaces based on integral equation algorithms," *IEEE Transactions on Antennas and Propagation*, vol. 55, no. 12, pp. 3460–3468, 2007.

[21] J. L. A. Quijano and G. Vecchi, "Field and source equivalence in source reconstruction on 3d surfaces," *Progress In Electromagnetics Research*, vol. 103, pp. 67–100, 2010.

[22] C. G. Parini, S. F. Gregson, and A. K. Brown, "Untethered near-field drone-based antenna measurement system for microwave frequencies using multiple reference antennas for phase and drone location recovery," *IET Microwaves, Antennas & Propagation*, vol. 16, no. 13, pp. 798–811, 2022. [Online]. Available: https://ietresearch.onlinelibrary.wiley.com/doi/abs/10.1049/mia2.12295

[23] D. Ostrzyharczik, J. Knapp, J. Kornprobst, and T. F. Eibert, "Inverse source solutions with huygens' surface conforming distributed directive spherical harmonics expansions," *IEEE Transactions on Antennas and Propagation*, vol. 71, no. 2, pp. 1684–1696, 2023.

[24] T. F. Eibert, D. Ostrzyharczik, J. Kornprobst, and J. Knapp, "On the generation of distributed spherical harmonics expansions for inverse source solutions," in *2023 17th European Conference on Antennas and Propagation (EuCAP)*, 2023, pp. 1–5.

[25] M. G. Fernández, Y. Álvarez López, and F. L.-H. Andrés, "Advances in antenna measurement and characterization using unmanned aerial vehicles," in *2019 13th European Conference on Antennas and Propagation (EuCAP)*, 2019, pp. 1–5.

[26] Y. Alvarez, F. Las-Heras, and M. R. Pino, "The sources reconstruction method for amplitude-only field measurements," *IEEE Transactions on Antennas and Propagation*, vol. 58, no. 8, pp. 2776–2781, 2010.

[27] S. F. Razavi and Y. Rahmat-Samii, "A new look at phaseless planar near-field measurements: limitations, simulations, measurements, and a hybrid solution," *IEEE Antennas and Propagation Magazine*, vol. 49, no. 2, pp. 170–178, 2007.

[28] A. Bangun, C. Culotta-López, A. Behboodi, R. Mathar, and D. Heberling, "On phaseless spherical near-field antenna measurements," in *2019 13th European Conference on Antennas and Propagation (EuCAP)*, 2019, pp. 1–5.

[29] B. Fuchs, M. Mattes, S. Rondineau, and L. Le Coq, "Phaseless near-field antenna measurements from two surface scans — numerical and experimental investigations," *IEEE Transactions on Antennas and Propagation*, vol. 68, no. 3, pp. 2315–2322, 2020.

[30] F. Rodríguez Varela, J. Fernandez Álvarez, B. Galocha Iragüen, M. Sierra Castañer, and O. Breinbjerg, "Numerical and experimental investigation of phaseless spherical near-field antenna measurements," *IEEE Transactions on Antennas and Propagation*, vol. 69, no. 12, pp. 8830–8841, 2021.

[31] S. Rengarajan and Y. Rahmat-Samii, "The field equivalence principle: illustration of the establishment of the non-intuitive null fields," *IEEE Antennas and Propagation Magazine*, vol. 42, no. 4, pp. 122–128, 2000.

[32] C. Ma, X. Liu, and Z. Wen, "Globally convergent levenberg-marquardt method for phase retrieval," *IEEE Transactions on Information Theory*, vol. 65, no. 4, pp. 2343–2359, 2019.

[33] N. Mézières, L. Le Coq, and B. Fuchs, "Phaseless spherical near-field antenna measurements with reduced samplings," *IEEE Transactions on Antennas and Propagation*, vol. 71, no. 9, pp. 7447–7456, 2023.

[34] T. Brown, I. Jeffrey, and P. Mojabi, "Multiplicatively regularized source reconstruction method for phaseless planar near-field antenna measurements," *IEEE Transactions on Antennas and Propagation*, vol. 65, no. 4, pp. 2020–2031, 2017.

[35] O. Bucci, C. Gennarelli, and C. Savarese, "Representation of electromagnetic fields over arbitrary surfaces by a finite and nonredundant number of samples," *IEEE Transactions on Antennas and Propagation*, vol. 46, no. 3, pp. 351–359, 1998.

[36] F. D'Agostino, F. Ferrara, C. Gennarelli, G. Gennarelli, R. Guerriero, and M. Migliozzi, "On the direct non-redundant near-field-to-far-field transformation in a cylindrical scanning geometry," *IEEE Antennas and Propagation Magazine*, vol. 54, no. 1, pp. 130–138, 2012.

[37] J. Laviada and F. Las-Heras, "Phaseless antenna measurement on non-redundant sample points via leith-upatnieks holography," *IEEE Transactions on Antennas and Propagation*, vol. 61, no. 8, pp. 4036–4044, 2013.

[38] F. Bevilacqua, A. Capozzoli, C. Curcio, F. D' Agostino, F. Ferrara, C. Gennarelli, R. Guerriero, A. Liseno, and M. Migliozzi, "A phaseless near-field to far-field transformation with planar wide-mesh scanning accounting for planar probe positioning errors," *IEEE Access*, pp. 1–1, 2023.

[39] L. Ciorba, F. Paonessa, M. Righero, G. Giordanengo, G. Virone, and G. Vecchi, "Radiation physics allows ten-fold optimization of UAV near-field scanning," in *2023 17th European Conference on Antennas and Propagation (EuCAP)*, 2023, pp. 1–4.

[40] A. D. Yaghian, "An Overview of Near-Field Antenna Measurements," *IEEE Transactions on Antennas and Propagation*, vol. 34, pp. 30 – 45, 1986.

[41] W. A. Mahmoud, A. S. Hadi, and T. M. Jawad, "Development of a 2-D wavelet transform based on kronecker product," *Al-Nahrain Journal of Science*, vol. 15, no. 4, pp. 208–213, Dec. 2012. [Online]. Available: https://anjs.edu.iq/index.php/anjs/article/view/627

[42] M. Francis, "Aperture-sampling requirements [and reply]," *IEEE Antennas and Propagation Magazine*, vol. 39, no. 5, pp. 76–81, 1997.

[43] D. W. Hess, "Historical background on the use of equivalent stray signal in comparison of antenna patterns," in *Proceedings of the 5th European Conference on Antennas and Propagation (EUCAP)*, 2011, pp. 2522–2526.

[44] R. Chandra, Z. Zhong, J. Hontz, V. McCulloch, C. Studer, and T. Goldstein, "Phasepack: A phase retrieval library," *Asilomar Conference on Signals, Systems, and Computers*, 2017.

[45] "IEEE recommended practice for near-field antenna measurements," *IEEE Std 1720-2012*, pp. 1–102, 2012.

[46] P. Petre and T. Sarkar, "Planar near-field to far-field transformation using an equivalent magnetic current approach," *IEEE Transactions on Antennas and Propagation*, vol. 40, no. 11, pp. 1348–1356, 1992.

YURI ÁLVAREZ LÓPEZ received the M.S. and Ph.D. degrees in telecommunication engineering from the University of Oviedo (Spain), in 2006 and 2009, respectively, both with Honors. He was a Visiting Scholar at Syracuse University, in 2008; a Visiting Postdoc at Northeastern University, Boston, USA, from 2011 to 2014; and a Visiting Postdoc at ELEDIA Research Center, Trento, Italy, in 2015. He has been with the Signal Theory and Communications research group of the University of Oviedo (Gijón, Spain) since 2006, where he is currently an Associate Professor. He is the Deputy Dean for Internationalization of the Polytechnic School of Engineering of Gijón, University of Oviedo. He has co-authored over 50 publications in first quartile-ranked scientific journals in the areas of antennas and propagation, electromagnetic imaging, nondestructive testing, and location and tracking systems. His research interests include antenna diagnostics, antenna measurement techniques, methods and techniques for indoor location based on Internet-of-Things networks, inverse scattering and imaging techniques for nondestructive testing applications, and phaseless methods for antenna diagnostics and imaging. Dr. Alvarez was the recipient of the 2011 Regional and National Awards for the Best Ph.D. Thesis on Telecommunication Engineering (category: security and defense), the Best Propagation Paper Award at the 2014 European Conference on Antennas and Propagation, and was part of the team awarded with the Idea of the Year at the 2019 GALILEO Masters Awards, European Global Navigation Satellite System Agency (GSA).

MARÍA GARCÍA FERNÁNDEZ(Member, IEEE) received the MSc and PhD degrees in telecommunication engineering from the University of Oviedo (Spain) in 2016 and 2019, respectively. She also received the BSc in Mathematics from National University of Education at Distance - UNED (Spain) in 2023. From 2013 to 2022 she was with the Signal Theory and Communications Research Group, TSC-UNIOVI, University of Oviedo. She was also a Visiting Student with Stanford University (Palo Alto, CA, USA) in 2013 and 2014, a Visiting Scholar with the Gordon Center for Subsurface Sensing and Imaging Systems, Northeastern University (Boston, MA, USA) in 2018, and a Visiting Researcher with the Radar Department of TNO (The Hague, The Netherlands) in 2019. In 2022, she joined Queen's University Belfast (United Kingdom), where she is currently a Marie Skłodowska-Curie Actions Research Fellow with the Centre for Wireless Innovation, CWI. She has authored more than 60 peer-reviewed journals and conference papers, and she holds two patents. Her current research interests include radar systems, computational imaging, inverse scattering, remote sensing, antenna measurement and diagnostics, and non-invasive measurement systems on board unmanned aerial vehicles. She has also received several awards, such as the 2020 National Award to the Best PhD Thesis on telecommunication engineering. She has been appointed as 2024 Young Professional Ambassador of the IEEE Antennas and Propagation Society..

JAIME LAVIADA MARTÍNEZwas born in Gijon, Spain. He received the M.S. degree in telecommunication engineering and the Ph.D. degree from the Universidad de Oviedo, Gijon, Spain, in 2005 and 2010, respectively. In 2006, he joined the research group Signal Theory and Communications, Universidad de Oviedo, where he has been involved in multiple national and European projects as well as contracts with several companies. In 2015, he moved to the Antennas Group, Universidad Publica de Navarra, Pamplona, Spain, with a National Post-Doctoral Fellowship collaborating in several applied research projects. He moved back to the Universidad de Oviedo, where he is currently an Associate Professor. In addition, he was a Visiting Scholar with the Electromagnetics and Communications Laboratory, Pennsylvania State University, State College, PA, USA, in 2007 as well asin 2008, and the Applied Microwave Nondestructive Testing Laboratory, Missouri S&T, Rolla, MO, USA, in 2017. He has served as Associated Editor for the IEEE Access. His research interests include numerical techniques applied to EM imaging, antenna measurements, method of moments, and antenna pattern synthesis.

FERNANDO LAS-HERAS ANDRÉS(Senior Member, IEEE) received the M.S. (1987) and Ph.D. (1990) degrees in telecommunication engineering from the Technical University of Madrid (UPM), Spain. He was a National Graduate Research Fellow and hold a position of associate professor (1991-2000) with UPM. Since 2003, he holds a full professor position with the University of Oviedo, Spain, where he was Vice Dean for telecommunication engineering with the Technical School of Engineering, Gijón (2004-2008). Since 2001, he has been heading the research group Signal Theory and Communications, TSC-UNIOVI, at the Dept. of Electrical Engineering, University of Oviedo. He has been Visiting Lecturer with the National University of Engineering, Peru, and with ESIGELEC, France, and Visiting Researcher with Syracuse University, NY, in 2000. He held the Telefónica Chair on RF technologies at the University of Oviedo (2005-2015), he was member of the Science, Technology, and Innovation Council of Asturias (2010-2012) and he is President of the professional Association of Telecommunication Engineers at Asturias from 2017. He has been member of the Board of Directors of the IEEE Spain Section (2012-2015), member (2016-2019) and Vice President (2020-2022) of the Board of the Joint IEEE AP03MTT17 Spain Chapter. He has led and participated in several research projects and has authored over 250 articles published in indexed scientific journals on topics of electromagnetic direct and inverse problems with applications to antenna measurement, electromagnetic imaging, and localization, developing computational electromagnetics algorithms and technology on microwaves, millimeter waves, and THz frequency bands.